공학석사학위논문

# 슐리렌 기법 및 레일리 산란을 이용한 초음속 제트의 고주파 밀도 변화 계측

# Measuring high frequency density fluctuation induced by supersonic jet with Schlieren photography and Rayleigh scattering

2019년 8월


서울대학교 대학원

기계항공공학부

박 한 준

# 슐리렌 기법 및 레일리 산란을 이용한 초음속 제트의 고주파 밀도 변화 계측

**Measuring high frequency density fluctuation induced by supersonic jet with Schlieren photography and Rayleigh scattering**

**지도교수 황 원 태**

**이 논문을 공학석사 학위논문으로 제출함**

2019년 4월


**서울대학교 대학원**

**기계항공공학부**

**박 한 준**


**박한준의 공학석사 학위논문을 인준함**

2019년 6월

**위 원 장 _____최__해__천_____(인)**

**부위원장 _____황__원__태_____(인)**

**위 원 _____박__형__민_____(인)**

# Measuring high frequency density fluctuation induced by supersonic jet with Schlieren photography and Rayleigh scattering

Han June Park
Department of Mechanical & Aerospace Engineering
Seoul National University

## Abstract

In high speed transportation, supersonic jet flows can appear in the propulsion system. Vehicle power efficiency is correlated with the jet flow structure and its physical characteristics. Thus, it is important to understand supersonic jet flow structure, but these flows generally have high fluctuation components which are difficult to measure with traditional diagnostic techniques. Using non-intrusive optical diagnostics can solve this problem. In this paper, Schlieren photography and Rayleigh scattering were utilized to measure density fluctuations of a supersonic jet. The shockwave structure of an over-expanded supersonic jet at Mach 1.5 was first observed using Schlieren photography. Next, high frequency density fluctuations were measured using laser Rayleigh scattering with a sample rate of 250 million per second. The experiments were carried out for four different nozzle pressure ratio (NPR) cases. The unique shockwave structure of each case was quantitatively and qualitatively analyzed.

**Keyword:** Density fluctuation, Rayleigh scattering, Schlieren photography, Supersonic jet
**Student Number:** 2017 - 24872

# Table of Contents

Abstract ..... i

Contents ..... ii

List of Figures ..... iii

List of Tables ..... v

Nomenclature ..... vi

Chapter 1. Introduction ..... 1

Chapter 2. Experimental method ..... 5

2.1 Experimental setup ..... 5

2.2 Measurement techniques ..... 6

2.2.1 Schlieren photography ..... 6
2.2.2 Rayleigh scattering ..... 7

Chapter 3. Experimental results ..... 12

3.1 Schlieren photography ..... 12

3.1.1 Shockwave structure ..... 12
3.1.2 Oblique shock wave angle ..... 13

3.2 Rayleigh scattering ..... 14

3.2.1 Photon counting method ..... 14
3.2.2 Shockwave structure and density fluctuation correlation ..... 17

Chapter 4. Discussion ..... 32

4.1 Comparison of average and fluctuation density ..... 32

Chapter 5. Conclusion ..... 33

Bibliography ..... 34

Abstract in Korean ..... 36

# List of Figures

FIGURE 2.1 Schlieren photography setup ..... 9

FIGURE 2.2 Laser Rayleigh scattering setup ..... 9

FIGURE 2.3 Refractive deflection caused by density gradients ..... 10

FIGURE 2.4 Schlieren photography schematic. ..... 10

FIGURE 2.5 Knife edge function ..... 11

FIGURE 2.6 Rayleigh and Mie scattering spectral line shape ..... 11

FIGURE 3.1 Schlieren ensemble image and density gradient contour ..... 20

FIGURE 3.2 Shockwave structure in NPR 3.5 ..... 21

FIGURE 3.3 Laval nozzle flow regime ..... 22

FIGURE 3.4 Shockwave structure change as NPR increase ..... 23

FIGURE 3.5 Oblique shockwave. ..... 23

FIGURE 3.6 Shockwave angle comparison of analytical solution and Schlieren image ..... 24

FIGURE 3.7 PMT Tube operation in single photoelectron state ..... 25

FIGURE 3.8 PMT Tube signal output of high intensity light ..... 25

FIGURE 3.9 PMT Tube signal output of low intensity light ..... 26

FIGURE 3.10 Raw signal of PMT Tube and noise source .....26

FIGURE 3.11 Histogram and Gaussian distribution of photon count.....27

FIGURE 3.12 Calibration curve between density and photon count .....27

FIGURE 3.13 3.2 bar shockwave position.....28

FIGURE 3.14 Schlieren average pixel value in NPR 3.2 .....28

FIGURE 3.15 Normalized mean density in NPR 3.2.....29

FIGURE 3.16 Normalized root-mean-square density fluctuation in NPR 3.2.....29

FIGURE 3.17 Normalized mean density .....30

FIGURE 3.18 Normalized root-mean-square density fluctuation.....30

FIGURE 3.19 Mean density increase after shockwave.....31

FIGURE 3.20 Root-mean-square density fluctuation increase after shockwave. 31

# List of Tables

TABLE 3.1 Jet core density with isentropic relation .....27

# Nomenclature

| | |
|---|---|
| $NPR$ | Nozzle pressure ratio |
| $I_r$ | Detected Rayleigh scattering signal |
| $n$ | Number density |
| $l$ | Length of probe volume |
| $\Omega$ | Solid angle for detection |
| $C_0$ | Optical transmission efficiency |
| $\sigma_r$ | Rayleigh cross section for gas molecules |
| $\rho$ | Density |
| $\rho_s$ | Reference density |
| $I_{rs}$ | Reference Rayleigh scattering signal |
| $M1$ | Mach number 1 |
| $M2$ | Mach number 2 |
| $\beta$ | Wave angle |
| $\theta$ | Turning angle |
| $\kappa$ | Ratio of specific heat |
| $\bar{\rho}$ | Mean density |
| $\rho_j$ | Isentropic jet core density |
| $\rho_a$ | Ambient density |
| $\rho_{rms}$ | Root−mean−square density |
| $\sigma^2{}_N$ | Variance of photon count |
| $\sigma^2{}_{sh}$ | Variance of shot noise |
| $\sigma^2{}_p$ | Variance of light power fluctuation |
| $N$ | Photon count |
| $N_{avg}$ | Photon count average |

| | |
|---|---|
| $P_0$ | Nozzle pressure |
| $T_0$ | Nozzle temperature |
| $P_{amb}$ | Ambient pressure |
| $R$ | Universal gas constant |

# Chapter 1. Introduction

## 1.1. Research Background

There is a lot of interest nowadays in high speed transportation. Supersonic civilian flight had been successfully demonstrated with the Concorde program, and there is renewed interest in developing a new supersonic aircraft. To technically develop such a vehicle, vast amounts of testing needs to be conducted. However, although a lot of testing was held, there is a major problem in supersonic aircraft which is noise. High amplitude noise which makes people uncomfortable is the main issue in operating supersonic civilian aircraft. Since noise reduction was important, many studies was carried out, but there were two difficulties. First, there are few reliable measurement techniques for measuring unsteady turbulent compressible flow. Second, it is hard to identify exact noise source within the supersonic jet. Theoretically, the source of the sound is known as turbulence fluctuations. Supersonic jets also produce shock-associated noise which is special case of noise. In this study, we focus on the first difficulty.

## 1.2. Measurement techniques

Velocity, pressure, temperature, and density are all significant parameters that must be analyzed to properly characterize the flow. However, due to harsh environment such as high speed and pressure,

measuring accurate physical quantities of the flow is extremely difficult.

When measuring physical quantities of the flow, intrusive measurement techniques have traditionally been utilized. For example, thermocouples and pitot tubes are often used for temperature and velocity measurement. However, there are three critical drawbacks of intrusive measurement techniques for high speed flow. First, interference of the probe with the flow causes errors. Second, intrusive probes are not suitable for harsh environments such as high pressure combustion. Third, most systems have low temporal resolution.

To resolve these problems, we can utilize non-intrusive optical diagnostics, which do not affect the flow and can sample with high temporal resolution. In this research, Schlieren photography and Rayleigh scattering were utilized to measure density fluctuations of a supersonic jet.

## 1.3. Literature Survey

There have been many previous studies about measuring physical properties of supersonic jet. Studies can be divided into two parts. First part is when the experiment tools were traditional such as hotwire or microphone. Morrsion [1] and Mclaughlin [2] successfully used hotwire for measurement at low Reynolds number, but at high Reynolds number the hotwire continued to break. Seiner & Reethof [3] also used hotwire but because of flow fluctuation, hot

wire probes produced noise. Intrusive microphone was used to measure pressure fluctuation by Armstrong [4] in supersonic jet. They stated the difficulty of measurement as Mach number increases. Stationary wave occurred which makes measurement error. Hurdle [5] also used microphone to measure acoustic wave. Intrusive microphone caused noise which made measurements difficult.

More recently, non-intrusive optical diagnostics were utilized for measuring physical properties. Lau [6] and Jiang [7] used laser Doppler velocimetry (LDV) to measure velocity fluctuation statistics. Although measurement was non-intrusive, there was critical biasing problems because of the seeding particle. Biasing problems happens also in particle image velocimetry (PIV). Schaffer [8] and Richarz [9] used LDV to measure velocity spectra. There were a lot of assumptions and approximations which impugned accuracy of measurement. Non-intrusive crossbeam technique was also used by Wilson [10] to measure density fluctuation. However, experiment assumption was valid in homogeneous turbulence, not in jet flow.

There were a few successful results which measured physical properties in supersonic jet. As mentioned previously, LDV and PIV have seeding particle difficulty in supersonic jet. If the seeding particle can be removed and only laser is used, accurate measurement can be accomplished. Panda [11] and Mercier [12] used Rayleigh scattering where seeding particle is unnecessary in under-expanded supersonic jet and measured accurate density fluctuation. However, the measurement was only held for one regime of supersonic jet.

## 1.4. Research Objective

In the present study, density variations within an over-expanded supersonic jet were measured via Schlieren photography and laser Rayleigh scattering. Schlieren photography utilizes light refraction caused by density gradients, and laser Rayleigh scattering utilizes molecular scattering to measure density. Schlieren photography was used for observing shockwave structure of over-expanded supersonic jet at Mach 1.5. Next, Rayleigh scattering was utilized to measure high frequency density fluctuation with a sample rate of 250 million per second. The experiments were conducted for four different nozzle pressure ratio (NPR) to verify measurement system. Combining the two diagnostics, qualitative and quantitative high temporal resolution density fluctuations were measured within a supersonic jet.

# Chapter 2. Experimental method

## 2.1. Experimental setup

The setup for the experiment is shown in figure 2.1 and 2.2. Each optical diagnostic is respectively depicted. A Laval nozzle (Misumi ALVA N0=.2) was used to create the supersonic jet. The cross-sectional area ratio between outlet and throat is 1.16 which resulted in an exit Mach number of 1.5.

In the case of Schlieren photography, a 22.5mW He-Ne laser (Thorlabs HNL225RB) is used as the light source. A 1mm diameter beam was first expanded through a beam expander. It then passed through a diverging lens to create the desired 9mm diameter measurement area. The supersonic jet is injected in this area. After passing through this measurement area, the light propagates through a Schlieren head and knife edge. The knife edge is located at a focal length of 15cm from the Schlieren head. Schlieren images are detected with a high speed camera (Phantom V2640) at 25,000 fps.

For the laser Rayleigh scattering setup, a 5W CW laser (Dantec RayPower) is used as the light source. To increase the intensity of Rayleigh scattering, a focal lens is placed between the nozzle and the laser. The laser beam that passes over the nozzle exits into a beam dump. Rayleigh scattering is measured by a photomultiplier tube (Thorlabs PMT2102, 80 MHz), which is placed at a 90-degree

position to obtain the strongest intensity signal.

The PMT signal is captured by an oscilloscope (Teledyne LeCroy Wavesurfer 510), which has a bandwidth of 1GHz and sample rate of 250 million points per second.

Rayleigh scattering measurements are very sensitive to Mie scattering caused by particles and other random reflections. Thus, several anti-reflection barriers are installed to prevent random light from entering the PMT. The nozzle also reflects laser light, thus it was painted with black paint. A filter (Parker Pneumatic P3N FA28GSM) is used to remove fine dust particles and droplets from the jet.

The experiment is carried out under four different nozzle pressure ratio (NPR) conditions of 2.8, 3.2, 3.5, and 3.8.

## 2.2. Measurement techniques

### 2.2.1 Schlieren photography

Schlieren photography is a measurement technique that can visualize density gradients, which means it does not measure density directly. As shown in figure 2.3, Schlieren imaging utilizes a phenomenon in which the light path deflects when passing through a region where fluid density gradients exist [13].

To use this deflection phenomenon, light which is passing through the measurement area should be collimated by focus lens. After the measurement area, light pass another focus lens which is

called Schlieren head. Schlieren head makes light to focus on small area. If a knife edge is placed on this area, there is a section where the light is blocked and a section that passes through as shown in figure 2.4 and figure 2.5. Therefore, bright and dark areas appear in the image, depending on the intensity of light passing through. This technique measures density gradient rather than the density itself.

### 2.2.2 Rayleigh scattering

When light scatters from a particle or molecule, two types of modes exist: Mie and Rayleigh scattering. Since Mie and Rayleigh scattering are both elastic scattering, the wavelength of the light does not change.

Rayleigh scattering contains a variety of information, which can measure physical quantities such as temperature, pressure, and density. In the present experiment, Rayleigh scattering was utilized as a density measurement diagnostic. The Rayleigh scattering intensity $I_r$ can be expressed as follows [14].

$$I_r = C_0 \cdot I_0 \cdot \Omega \cdot l \cdot n \cdot \sigma_r \cdots\cdots\cdots\cdots Equation\ 2.1$$

This expression explains number of molecules $n$ which have cross section $\sigma_r$ per unit volume passing through a laser beam with intensity $I_0$ and collecting into $\Omega$ and probed in length $l$ which has optical transmission efficiency $C_0$.

If the species and the light source are fixed and the temperature is constant, the ratio of the measured Rayleigh scattering intensity $I_r$ and reference Rayleigh scattering $I_{rs}$ is the same as the ratio of unknown density $\rho$ and reference density $\rho_s$.

$$\frac{I_r}{I_{rs}} = \frac{\rho}{\rho_s} \cdots\cdots\cdots\cdots Equation\ 2.2$$

The difficulty with Rayleigh scattering arises when it is measured in situations where Mie scattering from particles is also present. As shown in figure 2.6, Mie scattering intensity is significantly stronger than the Rayleigh scattering intensity. Thus, in order to measure Rayleigh scattering, it is imperative to eliminate Mie scattering and additional reflections from the surroundings.

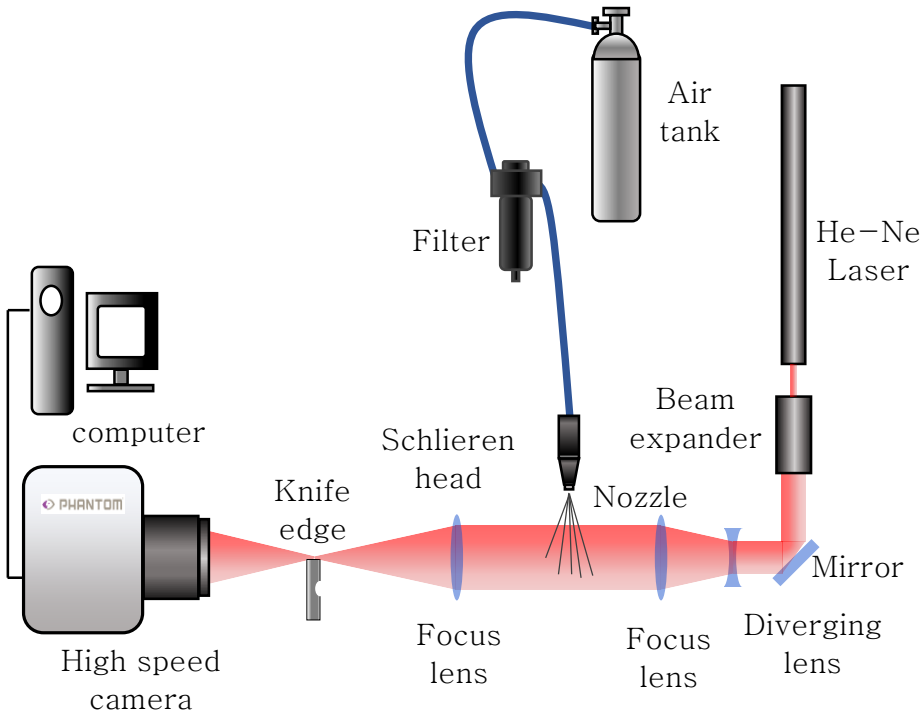


FIGURE 2.1 Schlieren photography setup

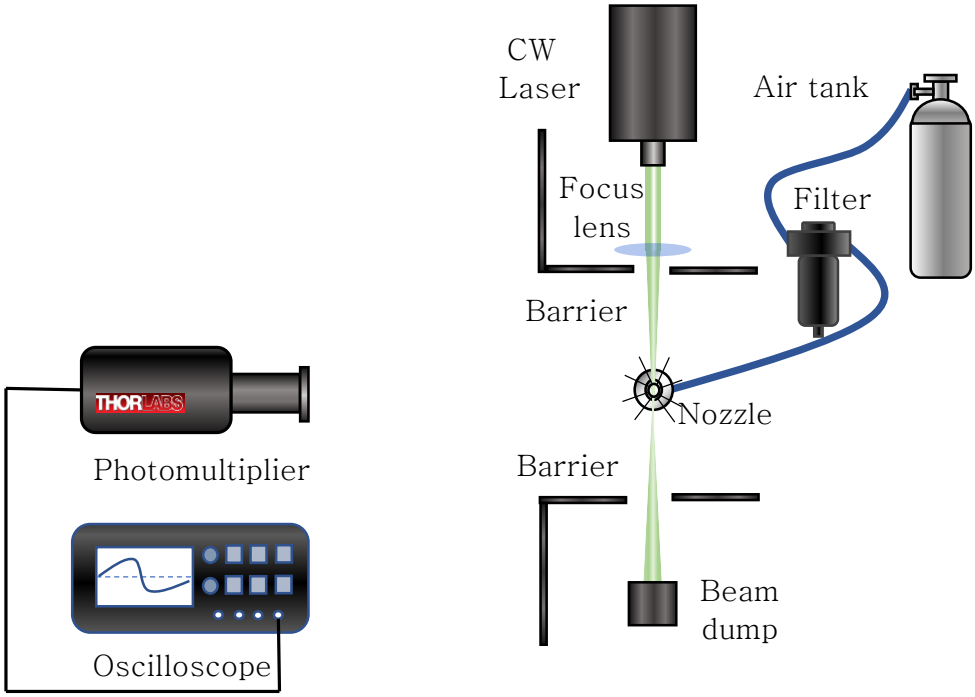


FIGURE 2.2 Laser Rayleigh scattering setup

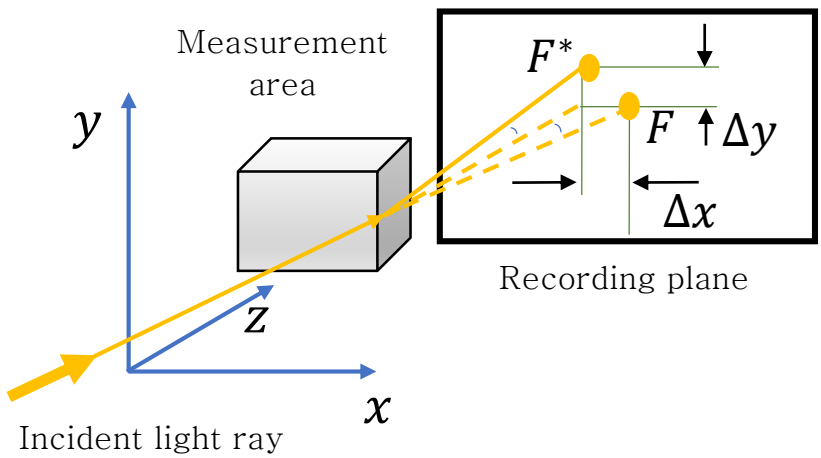


FIGURE 2.3 Refractive deflection caused by density gradients [13]

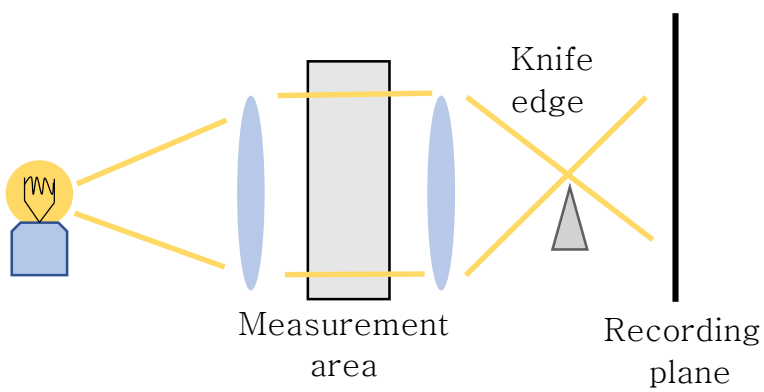


FIGURE 2.4 Schlieren photography schematic [13]

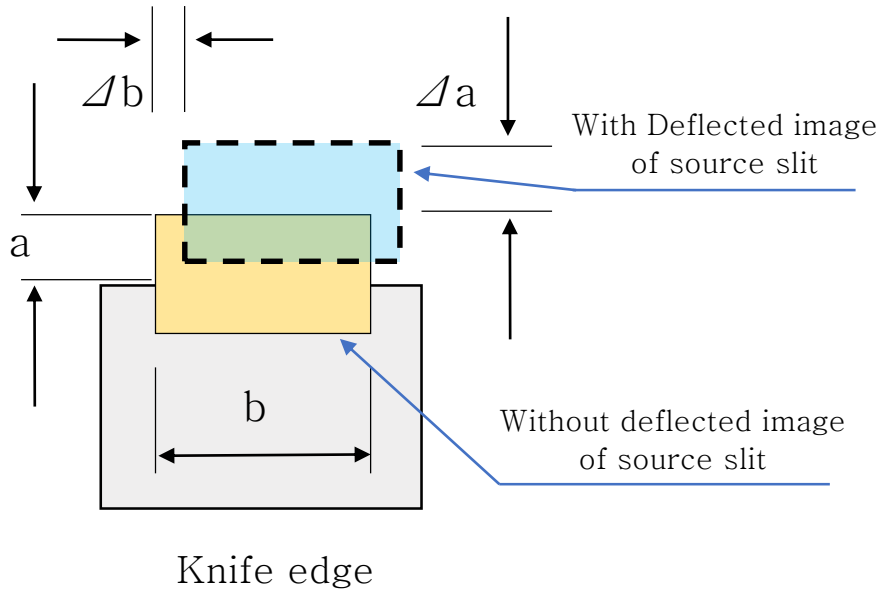


FIGURE 2.5 Knife edge function [13]

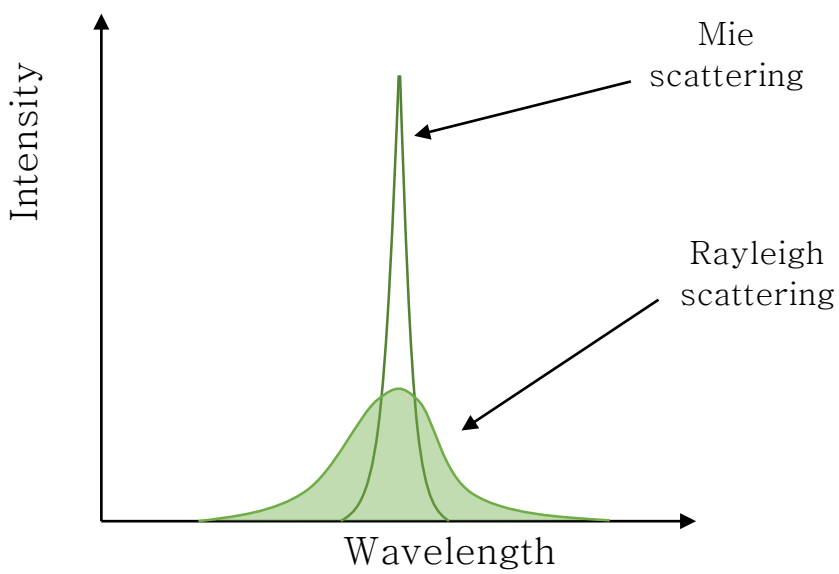


FIGURE 2.6 Rayleigh and Mie scattering spectral line shape

# Chapter 3. Experimental Results

## 3.1. Schlieren photography

### 3.1.1 Shockwave structure

The supersonic jet shockwave structure is obtained via Schlieren photography. Since shockwave is a phenomenon where density rises rapidly, Schlieren images can identify the shockwave structure via density gradients. This is demonstrated in figure 3.1. The top row images are raw Schlieren images. Bright and dark areas represent increasing and decreasing density, respectively. Bottom row images show intensity of density gradient with a color contour scale of 0 to 1.

A total of 4 cases with varying NPR were measured. Images are ensemble averages of 5000 pairs, obtained over 200ms. Flow structures including Mach disk, intercepting shock, reflected shock, and oblique shock can be identified in figures 3.1 and 3.2 from this typical Laval nozzle.

Especially, figure 3.2 shows detail of shockwave structure. At the exit, a pair of oblique shock exists. Then, each shock meets with a Mach disk and the Mach disk reflects the oblique shock. After the reflection, the reflected shock encounters the free jet boundary which changes the compression shock to an expansion fan. Expansion fans gather at the centerline and reflect off of each other. The

expansion fan changes into a compression shock after meeting with the free jet boundary. Following this the compression shock congregates downstream and expansion fan transitions to an intercepting shock. Then intercepting shock is reflected again similar to the previous oblique shock. This pattern happens periodically and the minimum pattern length is shock cell length.

### 3.1.2 Oblique shock wave angle

Typically, there are 4 regimes for a jet exiting a nozzle, as shown in figure 3.3. Each regime is determined by NPR and nozzle geometry. Since the nozzle cross-sectional area ratio between outlet and throat is 1.16, NPR 2.8 ~ 3.8 corresponds to the over-expanded regime. As NPR increases, a Mach disk develops where the oblique shocks meet, and after sufficient development the Mach disk disappears. This change of shock pattern is shown in figure 3.4

Considering the supersonic jet is in the over-expanded regime, the exit Mach number does not change. Instead, the wave angle of the oblique shock on the exit side changes depending on the pressure ratio. The oblique shockwave angle $\beta$ can be obtained from the outlet Mach number M1, specific heat ratio $\kappa$ and turning angle $\theta$ which is shown in figure 3.5.

$$\tan\theta = \cot\beta \ \frac{{M_1}^2 sin^2\beta - 1}{1 + \left(\frac{\kappa + 1}{2} - sin^2\beta\right){M_1}^2} \quad \cdots\cdots\cdots\cdots Equation\ 3.1$$

The analytically obtained angle and the angle obtained from the Schlieren images are compared with each other in figure 3.6. The difference is within 5°.

## 3.2. Rayleigh scattering

### 3.2.1 Photon counting method

Photomultiplier (PMT) is a light detecting device which is highly sensitive. Because of its high sensitivity, there are two signal modes in PMT: Analog and Digital mode. When the PMT detect the light, photon arrives at photocathode and electrons come out. Electrons multiply while passing through dynode. Finally, anode collects multiplied electrons as the output signal which is shown in figure 3.7. Each single photon can make individual pulse signal. In figure 3.8 and 3.9, it shows how PMT can be in two different modes. When PMT detects high intensity light, a lot of pulse overlap each other and makes analog signal. On the other hand, when PMT detects low intensity light, each individual pulse signal doesn't overlap and stay itself. Former mode is analog mode and latter mode is digital mode. In digital mode, light intensity can be measured in different method. Since the number of pulse signals is directly proportion to the light intensity, light intensity can be measured with the number of pulse signals. This method is called photon counting method.

As mentioned in experimental setup, quantitative density

fluctuation is measured with Rayleigh scattering which intensity of light is very low. In this condition, normal device like photodiode which measure the intensity of light with change in output signal value can be inaccurate. However, using high sensitivity device such as PMT which measures the intensity of light by counting the number of photons can provide accurate measurement.

In measuring Rayleigh scattering intensity, there are three major noise sources in photon counting method. Dark current, Mie scattering and shot noise. Dark current is low electric current that happens in photosensitive device like PMT although there are no photons. Mie scattering occurs due to dust particles. Even though filter is used, some of the dust particles exist to make high intensity pulse signals. Shot noise is the intrinsic noise of PMT because of randomness of photon arrival. The randomness causes shot noise to follow a Poisson distribution. Post-processing to eliminate dark current, high intensity Mie scattering and shot noise is needed.

Dark current and Mie scattering can be removed easily by lower bound and upper bound which is shown in figure 3.10. Collecting the count between two bounds is the Rayleigh scattering intensity including shot noise. Shot noise can be eliminated statistically because it follows a Poisson distribution. As the number of photon counts increases, the uncertainty of the Rayleigh scattering measurement decreases to the −0.5th power of the average count [15].

After post-processing, correlation between PMT photon count and fluid density was obtained. First, PMT photon count was quantified by following procedure. The raw signal was measured at sample rate of 250 million points per second for 20 ms. The number of sample was 5 million. The signal was divided into 1000 segments which make time interval 4 $\mu$s. Each segment has their own photon count and their distribution appears to be a Gaussian distribution as shown in figure 3.11. Next, fluid density was determined by using isentropic relation. Isentropic relation is available in only fully expanded regime until choking condition. Fluid density of jet core $\rho_j$ at nozzle exit can be calculated with Equation 3.2

$$\rho_j = \frac{P_0}{RT_o}\left(\frac{P_0}{P_{amb}}\right)^{-1/\kappa} \quad \cdots\cdots\cdots\cdots Equation\ 3.2$$

where $P_0$ is the nozzle pressure, $T_0$ is the nozzle temperature, $P_{amb}$ is the ambient pressure, $R$ is the universal gas constant and $\kappa$ is the ratio of specific heats.

3 case of fully expanded regime NPR 1.4, 1.6, 1.8 are calculated and results are shown in table 3.1. The linear correlation between mean of PMT photon count and fluid density can be expressed in

$$N = a\rho + b \quad \cdots\cdots\cdots\cdots Equation\ 3.3$$

where $N$ is photon count, $\rho$ is fluid density, $a$ is slope of line

constant and $b$ is background light intensity. As shown in figure 3.12, linear correlation corresponds with Rayleigh scattering theory fairly well.

### 3.2.2 Shockwave structure and density fluctuation correlation

Average and fluctuation density were measured at fifteen points total. Pointwise measurements were made at 1.5 mm resolution along the centerline. Figure 3.13 shows a schematic of the centerline. To be more quantitative, centerline pixel value of ensemble image is also shown in Figure 3.14. Pixel value trend can be compared with the average density $\bar{\rho}$ which is normalized as $(\bar{\rho}-\rho_a)/(\rho_j-\rho_a)$, and shown in figure 3.15. $\rho_j$ is the jet core density obtained from the isentropic relation and $\rho_a$ is ambient density. The average density varies with each pressure ratio depending on whether it is in the compression or expansion region. As shown in figure 3.15 and 3.16, a simple example is that as flow pass through the normal shockwave, the density increases. Then the density decreases until the next shockwave is encountered. The average density increases as Mach disk develops. And after Mach disk disappears, only oblique shock remains which make density fluctuation decrease. Along with the average density changes, shockwave structure also deforms. The shock cell length elongates as NPR increase. It is because NPR increment make flow stronger and results oblique shockwave angle lower. Lower angle causes longer reflection distance which makes

elongation of the shock cell length. These characteristics can be identified in figure 3.17.

The fluctuation density $\rho_{rms}$ is also normalized as $\rho_{rms}/(\rho_j - \rho_a)$. Normalized fluctuation density which is shown in figure 3.18 is obtained through Mandel's formula [16]. Mandel's formula explains that the variance of the photon count ${\sigma^2}_N$ is a sum of the variance of shot noise ${\sigma^2}_{sh}$ and the variance of light power fluctuation ${\sigma^2}_p$.

$$ {\sigma^2}_N = {\sigma^2}_{sh} + {\sigma^2}_p \quad \cdots\cdots\cdots\cdots Equation\ 3.4 $$

Shot noise follows Poisson statistics. Variance of shot noise is equal to photon count average, $N_{avg}$. Therefore, light power fluctuation can be calculated with Mandel's formula. Root-mean-square density fluctuation can be calculated through calibration curve slope constant $a$ and measurement temporal resolution $\Delta t$.

$$ \rho_{rms} = \sqrt{\frac{{\sigma^2}_p}{a^2 \Delta t^2}} \quad \cdots\cdots\cdots\cdots Equation\ 3.5 $$

The fluctuation density follows the same characteristics of the average density. When the flow encounters the shockwave, the fluctuation density increases. After passing through the shockwave, expansion region is reached and makes fluctuation density decrease. It is because the small zone of shockwave shakes rapidly more than

the large zone of expansion region. As NPR increases, elongation of the shock cell length can also be verified in figure 3.18. This can be explained similarly with average density. As NPR increases, oblique shockwave angle becomes lower which causes longer reflection distance and makes elongation of the shock cell length.

The density increase across the shockwave was compared with theory from oblique shock relations. The ratio of the mean density increase after normal shock and oblique shock can be calculated from equation 3.1 and figure 3.17. The result is shown in figure 3.19.

The fluctuation density cannot be calculated from equation 3.1, but the tendency shown in figure 3.20 demonstrates that the fluctuation density also follows the shockwave structure.

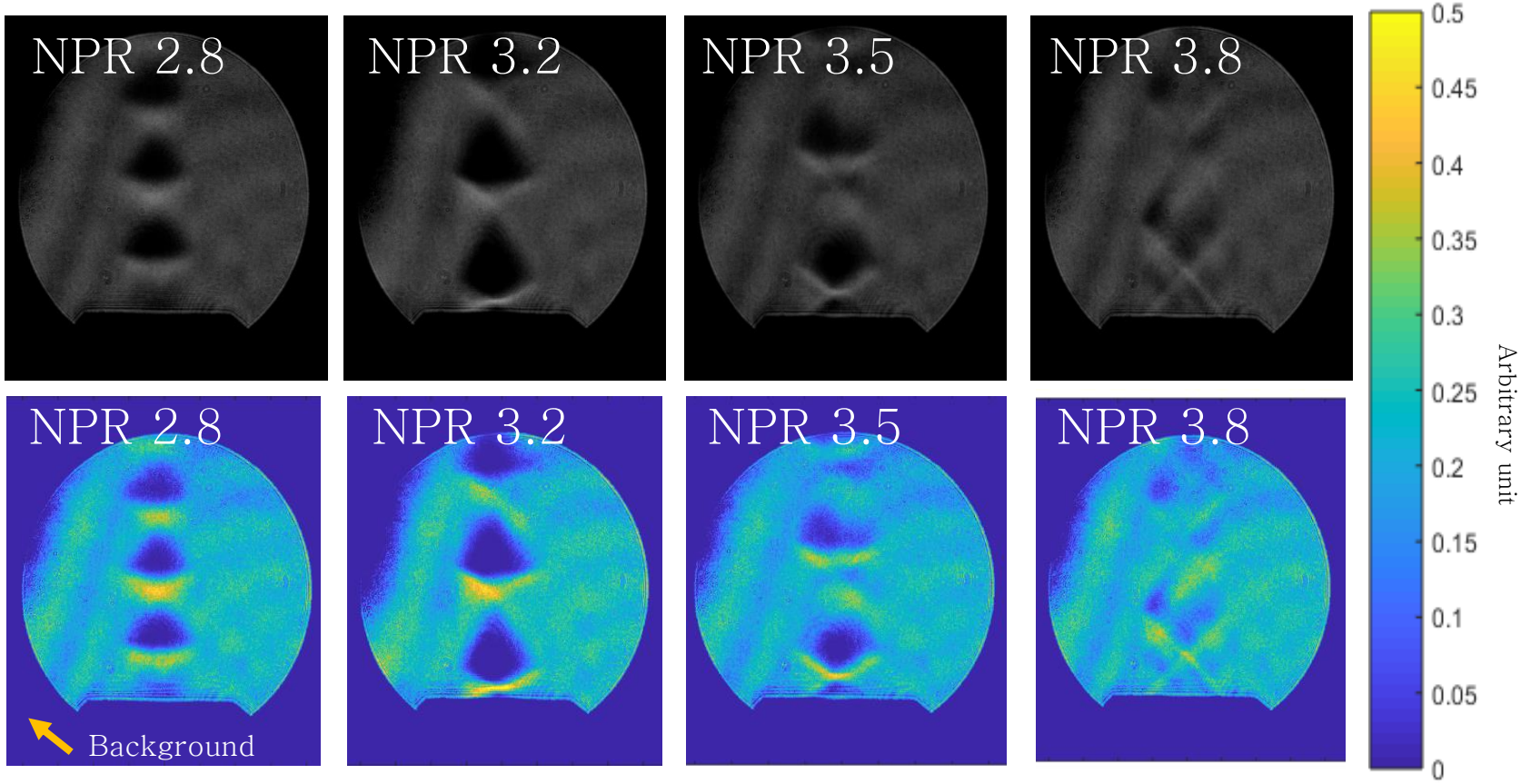


FIGURE 3.1 Schlieren image and density gradient contour

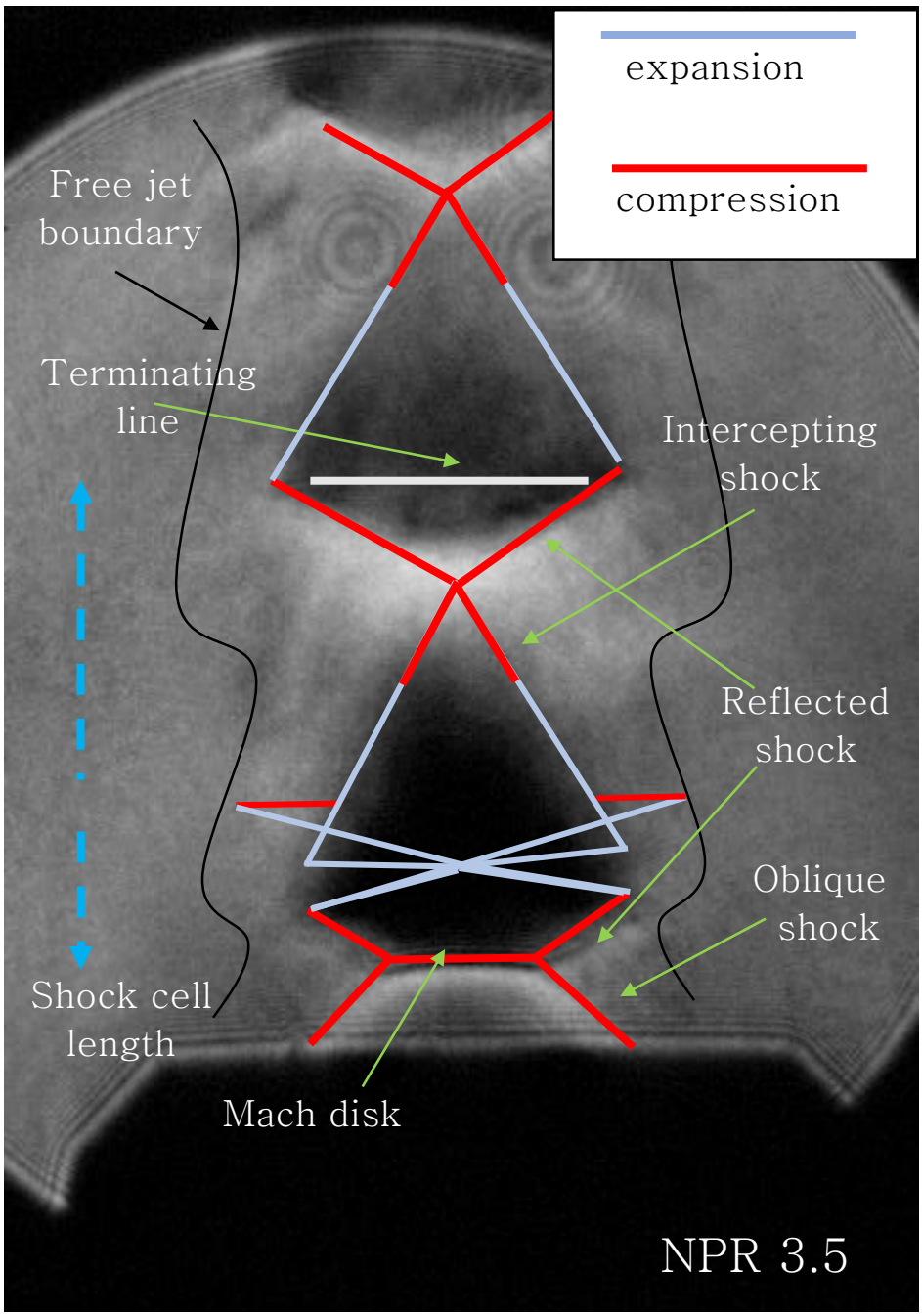


FIGURE 3.2 Shockwave structure in NPR 3.5

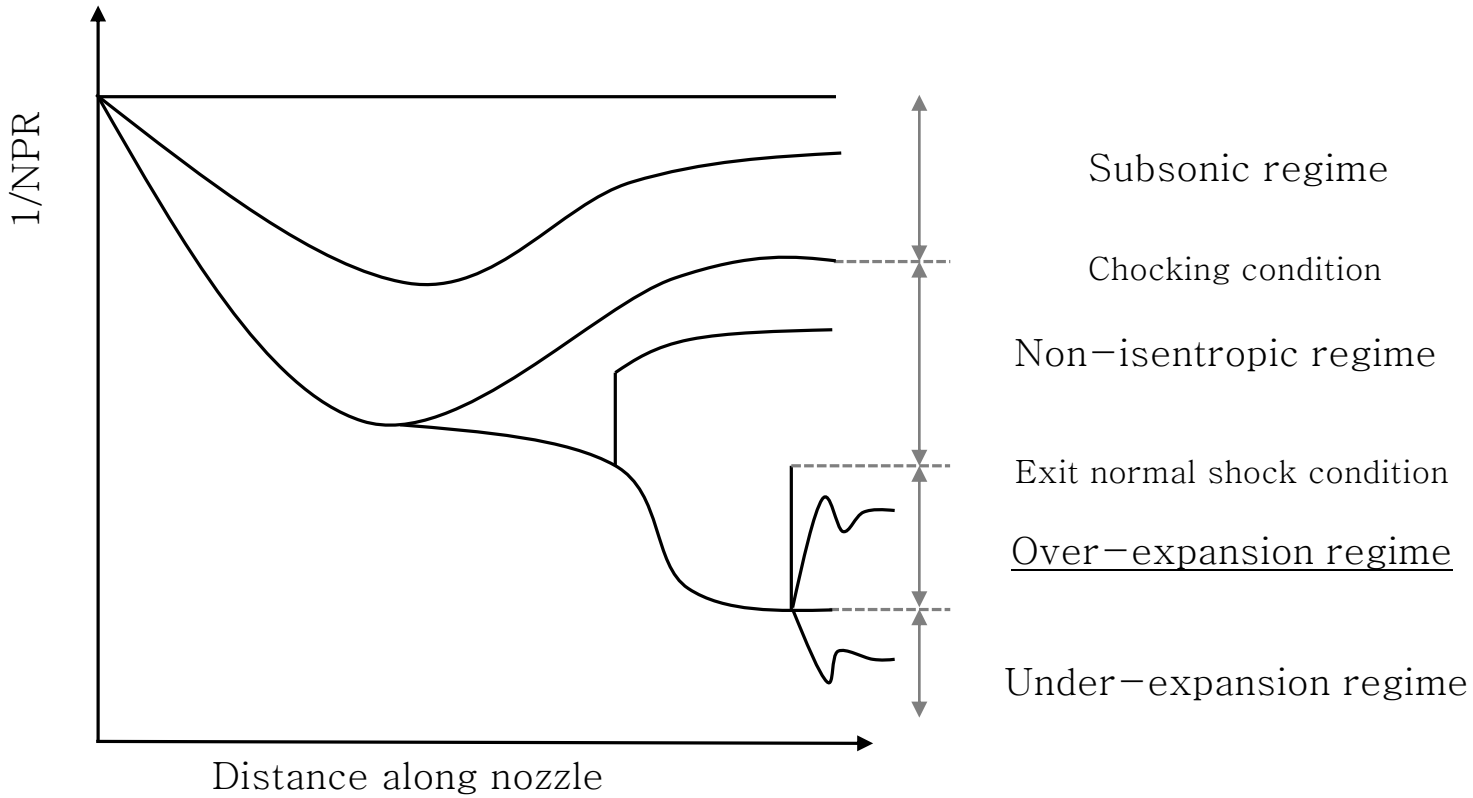


FIGURE 3.3 Laval nozzle flow regime

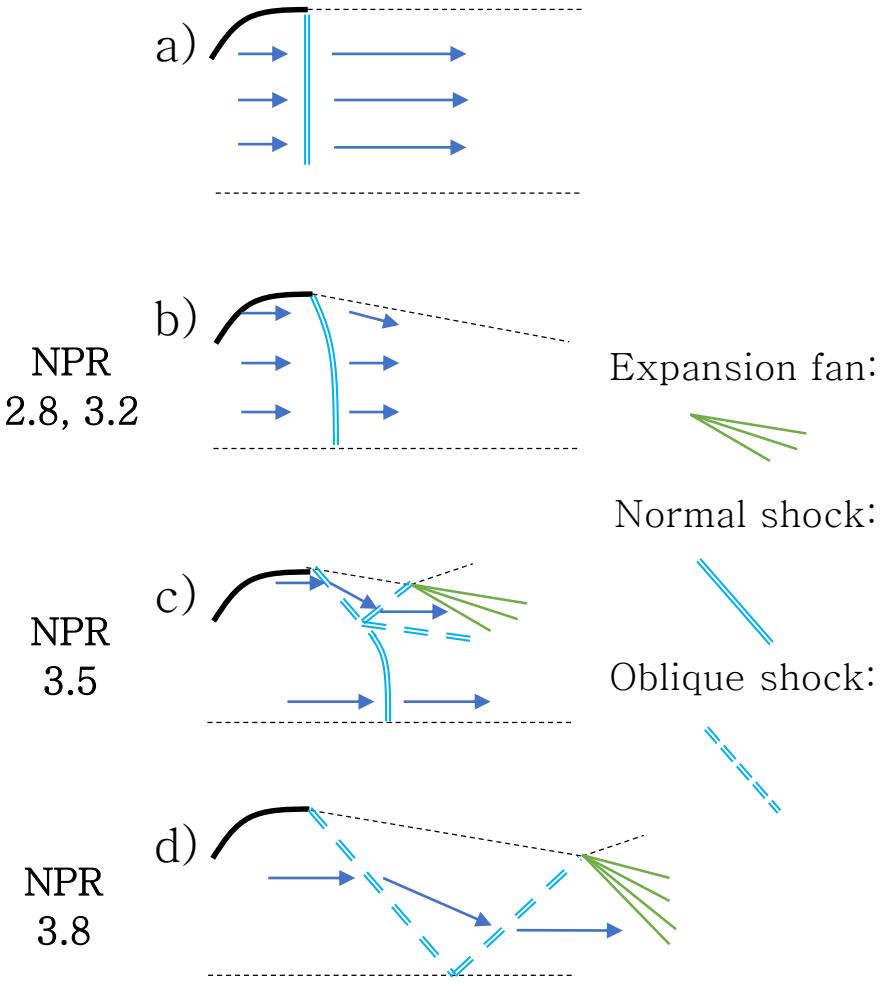


FIGURE 3.4 Shockwave structure change as NPR increase

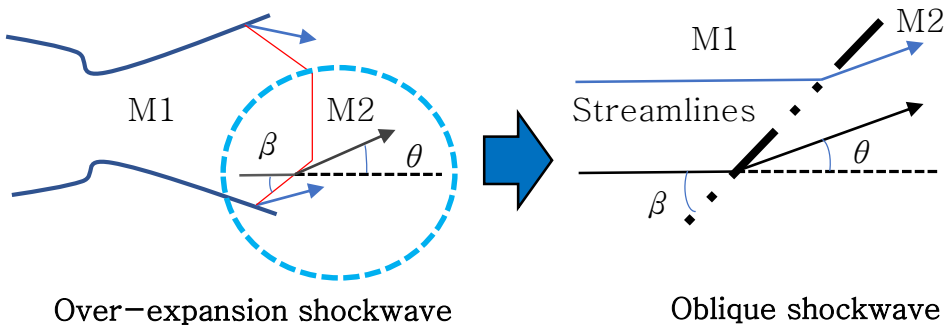


FIGURE 3.5 Oblique shockwave

a)

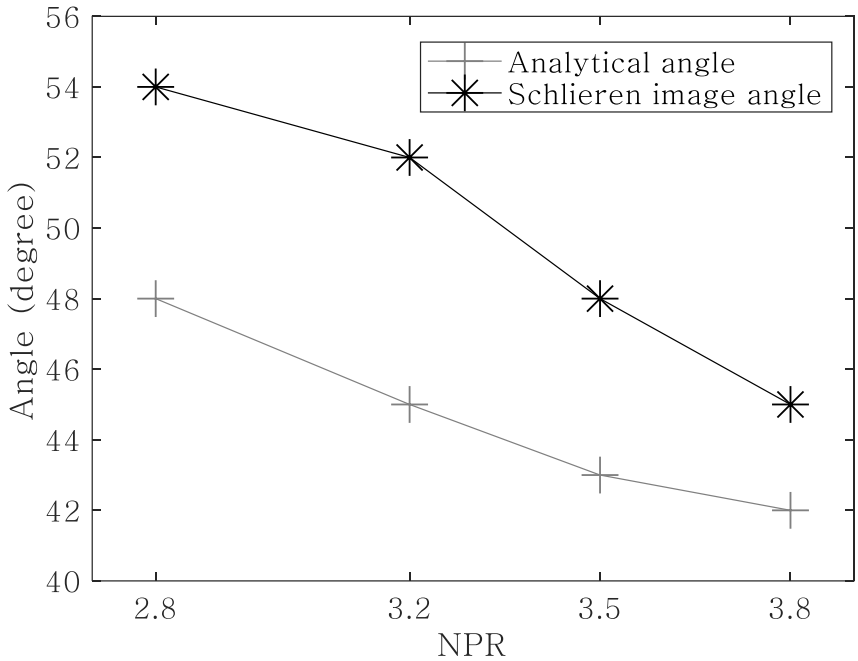


b)

| Area ratio : 1.16 / Mach number : 1.5 | | |
|---|---|---|
| NPR | Analytical (degree) | Schlieren (degree) |
| 2.8 | 48 | 54 |
| 3.2 | 45 | 52 |
| 3.5 | 43 | 48 |
| 3.8 | 42 | 45 |

FIGURE 3.6 Shockwave angle comparison of analytic solution and Schlieren image

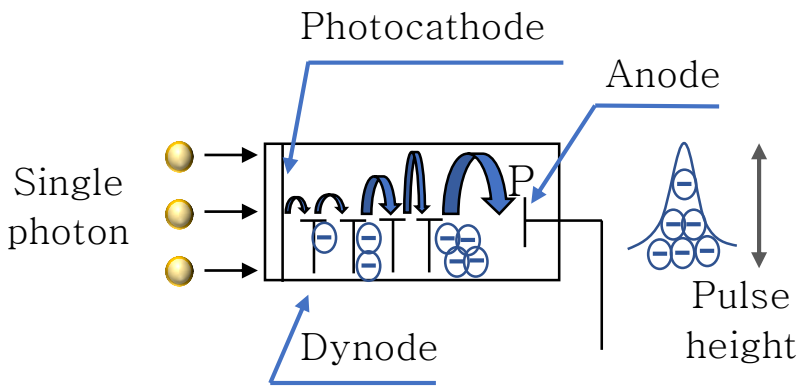


FIGURE 3.7 PMT Tube operation in single photoelectron state [15]

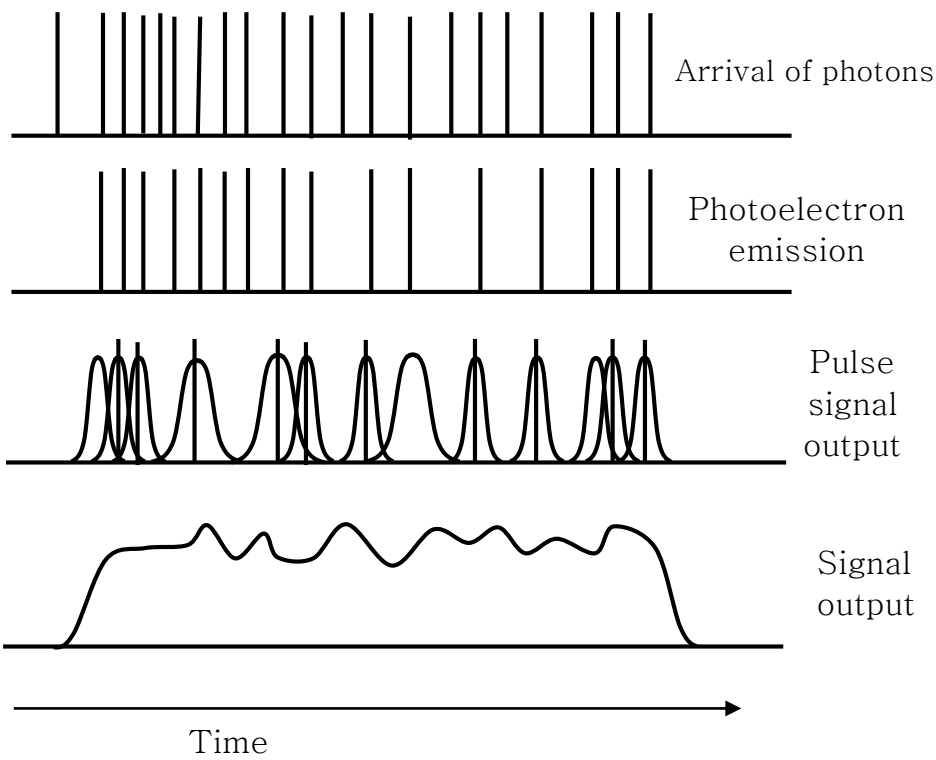


FIGURE 3.8 PMT Tube signal output of high intensity light [15]

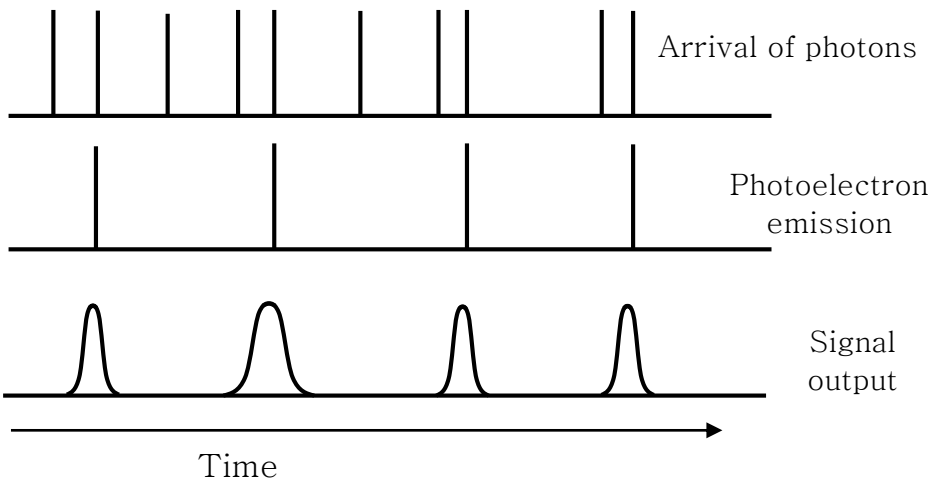


FIGURE 3.9 PMT Tube signal output of low intensity light [15]

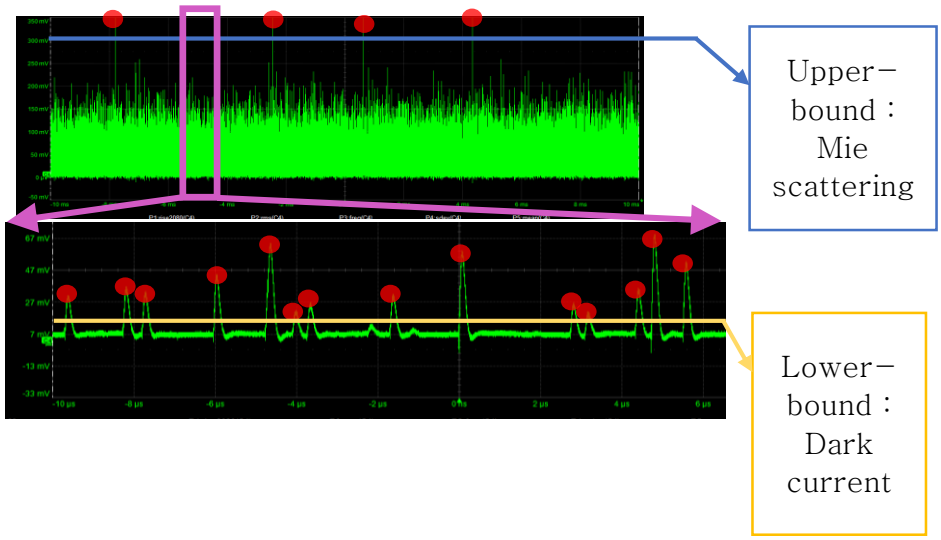


FIGURE 3.10 Raw signal of PMT Tube and noise source

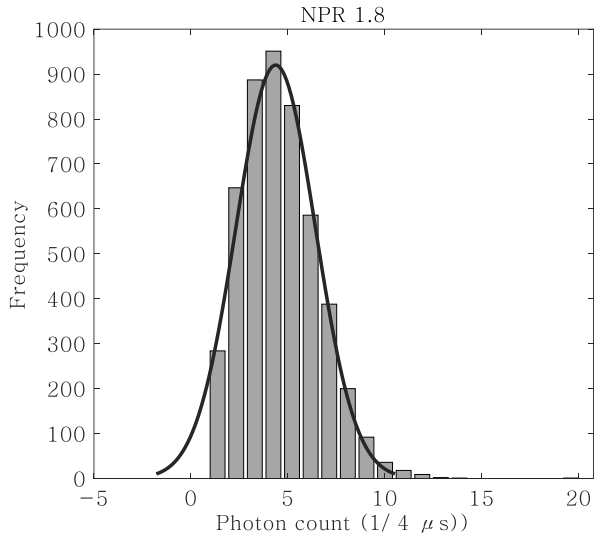


FIGURE 3.11 Histogram and Gaussian distribution of photon count

| NPR | Density |
|---|---|
| 1.4 | 1.35 $kg/m^3$ |
| 1.6 | 1.40 $kg/m^3$ |
| 1.8 | 1.45 $kg/m^3$ |

TABLE 3.1 Jet core density with isentropic realtion

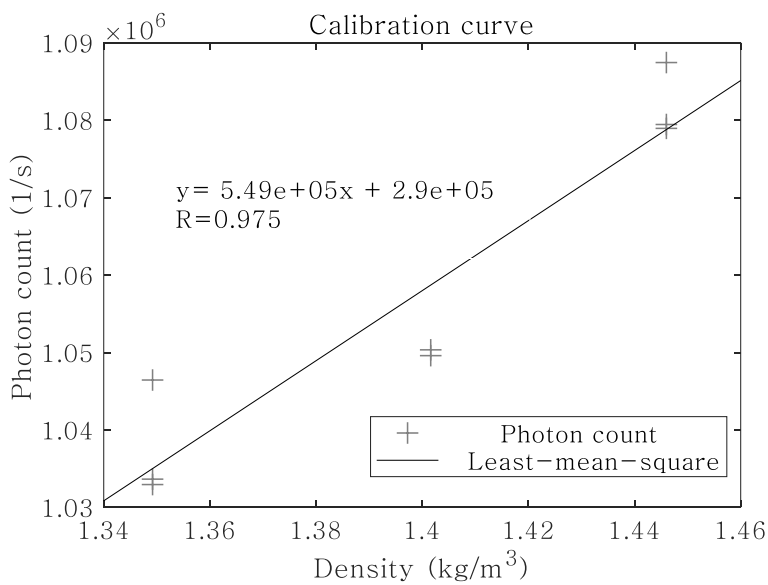


FIGURE 3.12 Calibration curve between density and photon count

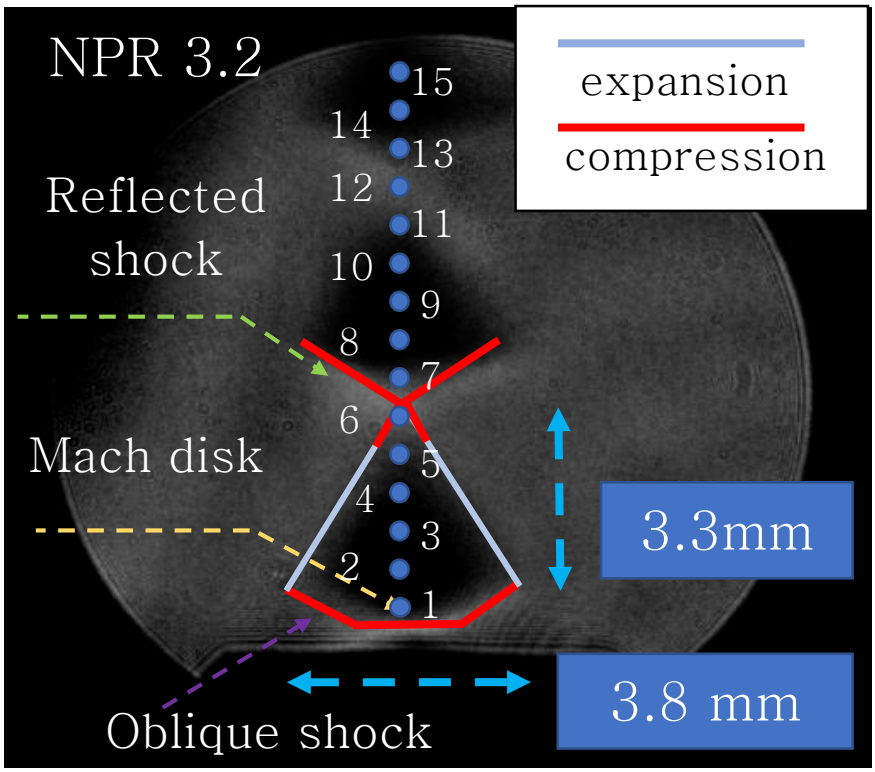


FIGURE 3.13 3.2 bar shockwave position

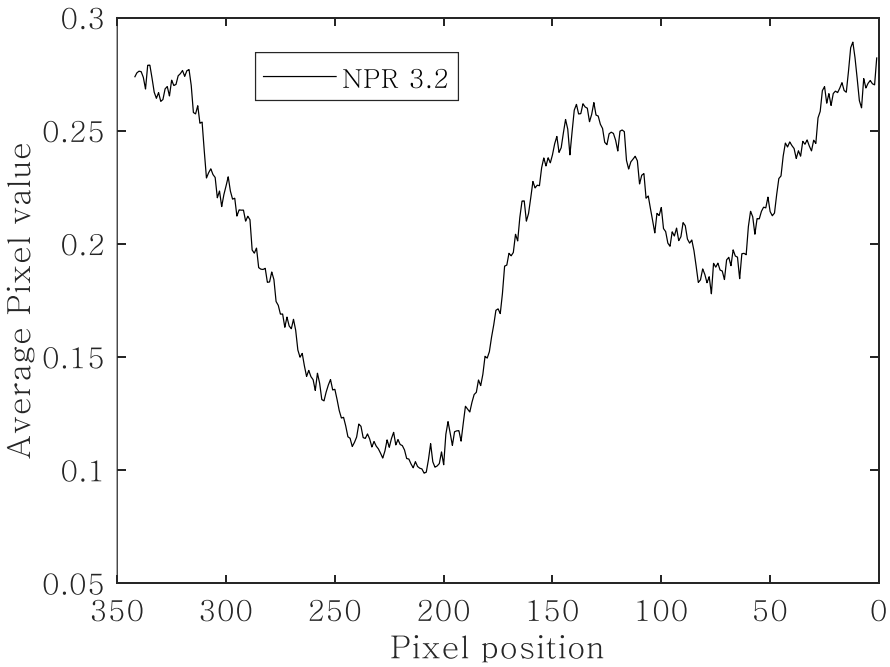


FIGURE 3.14 Schlieren average pixel value in NPR 3.2

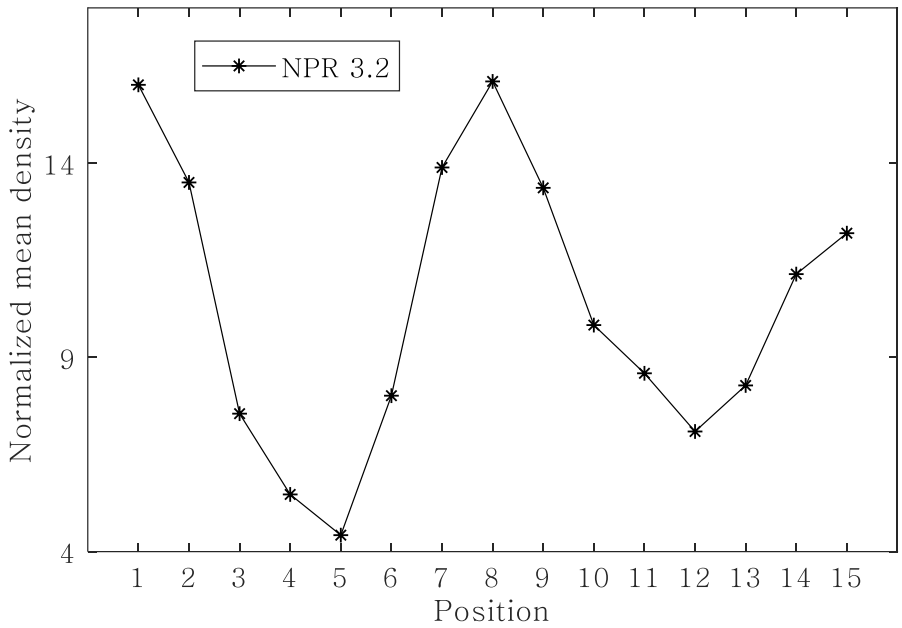


FIGURE 3.15 Normalized mean density in NPR 3.2

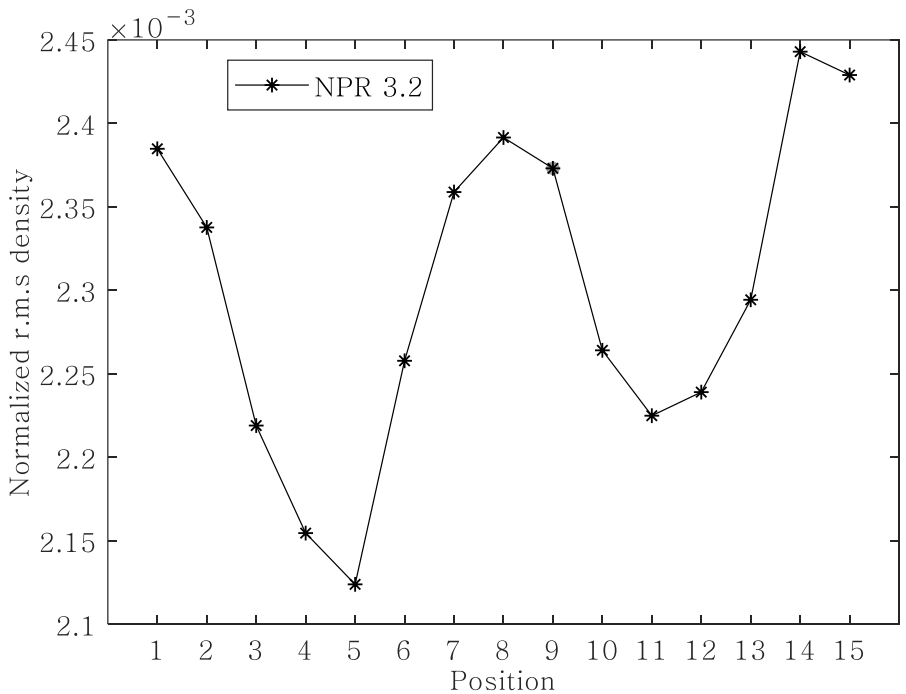


FIGURE 3.16 Normalized root−mean−square density fluctuation in NPR 3.2

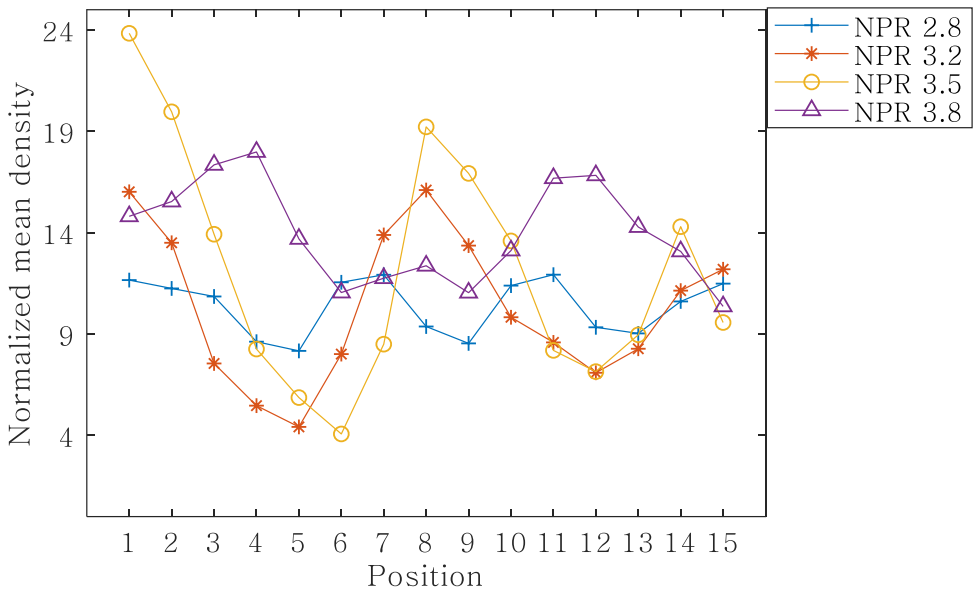


FIGURE 3.17 Normalized mean density

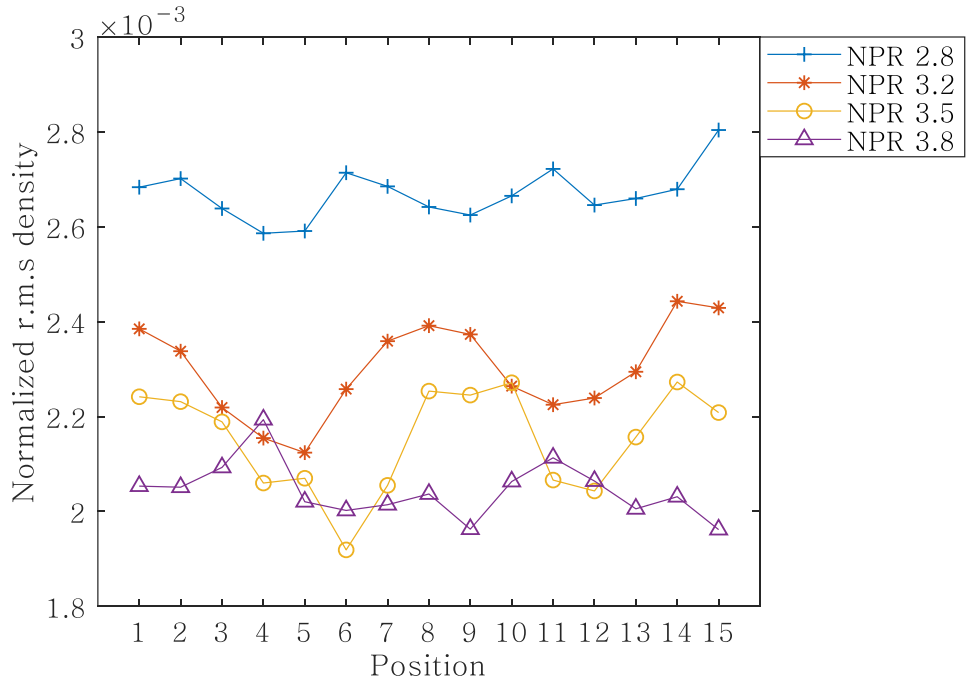


FIGURE 3.18 Normalized root−mean−square density fluctuation

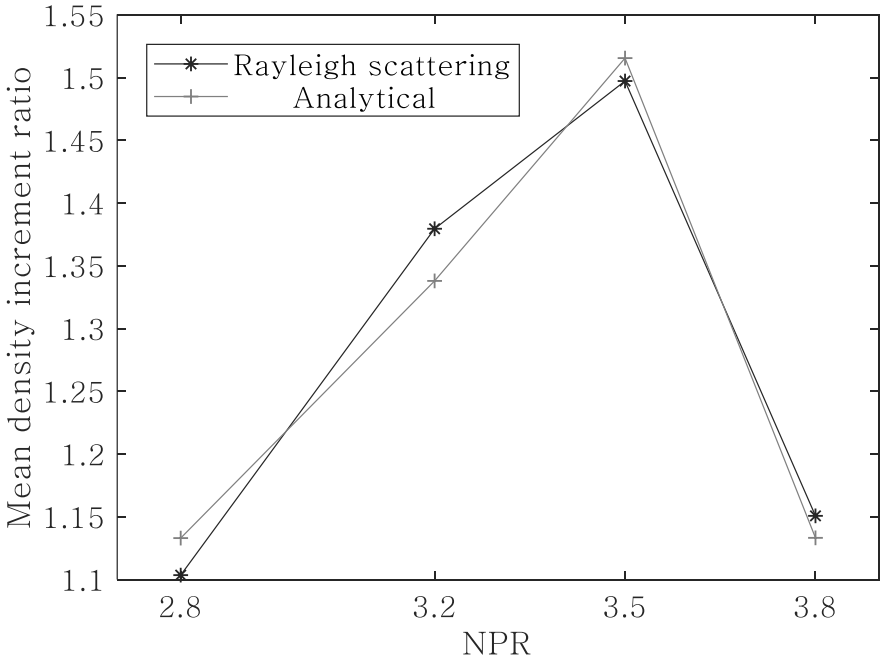


FIGURE 3.19 Mean density increase after shockwave

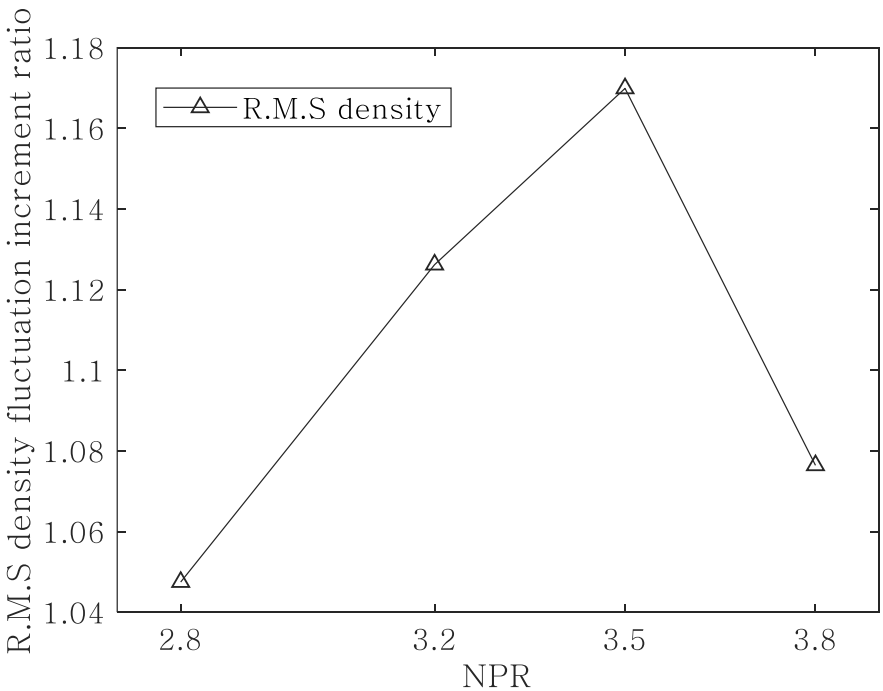


FIGURE 3.20 Root-mean-square density

fluctuation increase after shockwave

# Chapter 4. Discussion

## 4.1. Comparison of average and fluctuation density

From the experimental results, we found that the average density follows the shockwave structure. This tendency also appeared in fluctuation density. However, comparing average and fluctuation density, there is distinct difference between them. In figure 3.17 and 3.18, there is no specific trend in the range of average density as NPR increases. However, fluctuation density has distinct characteristic. As NPR increases, overall fluctuation density decreases.

The tendency of fluctuation density can be explained as follows. Although the shockwave structure deforms as NPR increases, the structure becomes more stable. This means the position of the shockwave becomes steadily stable and the position change of the shockwave is reduced. If the position of the shockwave causing the density change is stably maintained, overall fluctuation density decreases.

# Chapter 5. Conclusion

In the present study, shockwave structure and density fluctuations of a Mach 1.5 over-expanded supersonic jet was analyzed with Schlieren photography and Laser Rayleigh scattering.

The shockwave structure was verified by Schlieren photography and the structure with respect to pressure ratio was confirmed to be consistent with theory. Quantitative analysis for one shock cell length at high temporal resolution showed that the average density changes through the shock structure, as outlined in previous studies. The density fluctuations from the high-speed measurements also supported this observation.

# Bibliography


1. Morrison, G. and D. McLaughlin, *Noise generation by instabilities in low Reynolds number supersonic jets.* Journal of Sound and Vibration, 1979. **65**(2): p. 177-191.
2. McLaughlin, D.K., G.L. Morrison, and T.R. Troutt, *Experiments on the instability waves in a supersonic jet and their acoustic radiation.* Journal of Fluid Mechanics, 1975. **69**(1): p. 73-95.
3. Seiner, J. and G. Reethof. *On the distribution of source coherency in subsonic jets*. in *12th Aerospace Sciences Meeting*. 1974.
4. Armstrong, R.R., A. Michalke, and H. V. Fuchs, *Coherent structures in jet turbulence and noise.* AIAA Journal, 1977. **15**(7): p. 1011-1017.
5. Hurdle, P.M., W. Meecham, and B.K. Hodder, *Investigation of the aerodynamic noise generating region of a jet engine by means of the simple source fluid dilatation model.* The Journal of the Acoustical Society of America, 1974. **56**(6): p. 1708-1721.
6. Lau, J., *Effects of exit Mach number and temperature on mean-flow and turbulence characteristics in round jets.* Journal of Fluid Mechanics, 1981. **105**: p. 193-218.
7. Jiang, L.Y. and J.P. Sislian, *Velocity and density measurements in supersonic high-temperature exhaust plumes.* AIAA Journal, 1998. **36**(7): p. 1216-1222.
8. Schaffar, M., *Direct measurements of the correlation between axial in-jet velocity fluctuations and far field noise near the axis of a cold jet.* Journal of Sound and Vibration, 1979. **64**(1): p. 73-83.
9. Richarz, W., *Direct correlation of noise and flow of a jet using laser Doppler.* AIAA journal, 1980. **18**(7): p. 759-765.
10. Wilson, L. and R. Damkevala, *Statistical properties of turbulent density fluctuations.* Journal of Fluid Mechanics, 1970. **43**(2): p. 291-303.

11. Panda, J. and R.G. Seasholtz, *Experimental investigation of density fluctuations in high-speed jets and correlation with generated noise.* Journal of Fluid Mechanics, 2002. **450**: p. 97-130.
12. Mercier, B., et al., *Density Fluctuations Measurement by Rayleigh Scattering Using a Single Photomultiplier.* AIAA Journal, 2018. **56**(4): p. 1310-1316.
13. Tropea, C. and A.L. Yarin, *Springer handbook of experimental fluid mechanics*. Vol. 1. 2007: Springer Science & Business Media.
14. Miles, R.B., W.R. Lempert, and J.N. Forkey, *Laser Rayleigh scattering.* Measurement Science and Technology, 2001. **12**(5): p. R33-R51.
15. Hamamatsu Photonics, K., *Photomultiplier tubes: Basics and applications.* Edition 3a, 2007. **310**.
16. Bea, S. and M. Teich, *Fundamentals of Photonics.* Wiley, 1991: p. 313.

# 슐리렌 기법 및 레일리 산란을 이용한 초음속 제트의 고주파 밀도 변화 계측

서울대학교 대학원
기계항공공학부
박 한 준

## 요약

고속 수송체에서는 초음속 제트 유동이 추진 장치에 나타날 수 있다. 수송체 동력 효율은 제트 유동 구조 및 그 물리적 특정과 상관관계가 있다. 따라서 초음속 제트 유동 구조를 이해하는 것은 중요하다. 그러나, 일반적으로 이러한 유동은 전통적인 진단 기술로는 측정하기 어려운 높은 변동 요소를 가지고 있다. 이러한 문제는 비침입성 광학 진단을 이용하면 해결할 수 있으며, 이 논문에서는 슐리렌 기법과 레일리 산란을 이용하여 초음속 제트의 밀도 변화를 측정하였다. 먼저, 마하 1.5에서 과도하게 팽창된 초음속 제트의 충격파 구조를 슐리렌 기법으로 관찰하였다. 다음 초당 2억 5천만개 샘플 속도로 레이저 레일리 산란을 이용하여 고주파 밀도 변화를 측정하였다. 실험은 네 가지 다른 노즐 압력비 (NPR)의 경우에 대해 수행되었으며, 각 경우의 고유한 충격파 구조에 대해 정량적으로, 정성적으로 분석하였다.

주요어: 밀도 변화, 레일리 산란, 슐리렌 기법, 초음속 제트
학번: 2017-24872